SCATTERING OF ELECTRONS IN GRAZING INCIDENCE MIRROR TELESCOPES *

A. Hilgers[1] and P. Gondoin[2]

[1]*Space Environments and Effects Analysis Section,*
Technical and Operational Support Directorate
(http://www.estec.esa.nl/wmwww/wma/)
[2]Astrophysics Division, Space Science Department
European Space Research and Technology Centre, European Space Agency,
Noordwijk, The Netherlands, NL-2200 AG.

ABSTRACT

Magnetospheric and interplanetary electrons can cause problems to X-ray grazing incidence telescope since they can enter the mirror shells and further reach the detector or interact with them hereby producing X-ray emission. An analytical model is presented to evaluate these effects and is briefly compared to previous existing models. An upper bound of the expected level of particle induced background is derived using an electron flux model in the range 1 keV to several MeV derived from ISEE particle measurements and interplanetary measurements. This study suggests that energetic plasma environment monitoring method should be considered as a support to provide additional quality control of X-ray measurements.

Key words: Plasma sheet electrons; X-ray mirror.

1. INTRODUCTION

Soft X-ray telescopes using grazing incidence have specific optical mirror systems that are particularly sensitive to magnetospheric and interplanetary electrons. A sketch of such a mirror system is shown in Figure 1.

The interplanetary and magnetospheric electrons that are normally stopped by spacecraft walls can propagate between the mirror shells and either reach the detector in the focal plan or generate X-rays by impact on the shells. In both cases, if the electron energy is of the order of the energy of the photons for which the instrument is designed, the effect will contribute to an artificial X-ray background. The first effect has been investigated in previous studies either by assuming an X-ray type of propagation for the electrons [Danner, 1993] or through a complete Monte-Carlo simulation [Sumner et al. 1989; Sumner and Lieu, 1990] whereas the second effects seems to

not have been discussed in the literature up to now. In the present study an upper bound of the two effects is derived under the main assumption that the reflections of the electrons is specular. This hypothesis leads to simple analytical expressions that are upper bounds of the expected background and therefore suitable to engineering specifications. Finally, a model of the input electron flux is developed on the basis of ISEE-2 measurements. Current limitations of this electron model are discussed and a strategy for improving it is proposed.
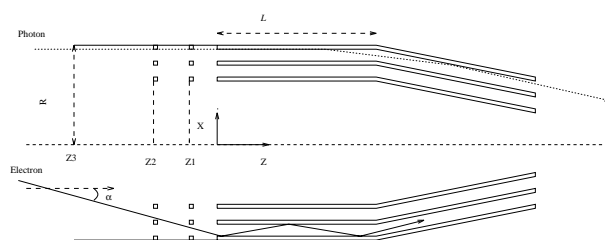

Figure 1. Sketch of a Wolter type mirror system of an X-ray telescope. The mirror shells located along positive Z values. They may be prolongated by a main baffle along negative Z values. Also additional X-ray baffles are located at $Z = Z_1$ and $Z = Z_2$ can be used in order to reduce the flux of non grazing angle photons.

2. ELECTRON PROPAGATION PROBABILITY WITHIN THE SHELLS

It is assumed that all reflections are specular but with a coefficient of reflection η depending of the angle of incidence θ and of the material according to *Shimizu* [1974]

$$\eta(\theta) = \exp(\text{Log}(\eta_0)\cos(\theta)) \tag{1}$$

Assuming that all electrons entering the shell system have their first impact at the entrance, the computation of the distribution of probability for an electron

to reach the depth z is rather straightforward and reduces to,

$$B(\alpha, w, z, i) = \exp\left(-\mu(z)\frac{\sin^2(\alpha)}{\cos(\alpha)}\right) \text{ if } z \leq L$$

(2)

and

$$B(\alpha, w, z, i) = \exp\left(-\mu(L)\frac{\sin^2(\alpha)}{\cos(\alpha)}\right.$$

$$\left. -\mu(x-L)\frac{\sin^2(\alpha \pm \gamma)}{\cos(\alpha \pm \gamma)}\right) \text{ if } z > L$$

where

$$\mu(s) = -\frac{s\text{Log}(\eta_0)}{2\delta}\cos\phi \quad (3)$$

In the above expressions, $\text{Log}(\eta_0)$ is the averaged value of the logarithmic of the reflection coefficient at normal incidence over the materials of each size of the shell, γ is the angle between the two shells, α is the angle between the particle velocity vector and the mirror optical axis and ϕ is the angle between the projection of the velocity vector in a plane perpendicular to the mirror axis and the perpendicular to the surface of the mirror at the impact location. In addition, the part of the flux reflected toward the mirror entrance due to the inclination γ of the second shell is neglected since γ is usually very small.

3. FLUX PARALLEL TO THE MIRROR AXIS

The electron flux parallel to the mirror axis at depth z can be written:

$$F_1 = \iiint g(w)\sin\alpha \, \cos\alpha A(\alpha, \phi, i)B(\alpha, w, z, i)d\phi d\alpha dw$$

(4)

where $g(w)$ is the differential flux of the particles with energy w (assuming an isotropic velocity distribution), $A(\alpha, \phi, i)$ is the density function of solid angle within which particles from the free space may access the mirror entrance, and $B(\alpha, w, z, i)$ is the density of probability that a particle entering the mirror system with a polar angle α propagates to the location z.

The term $\cos\alpha$ must actually be slightly modified for $z > L$ to take into account the division of the initial beam in 3 different beams with respective angle α, $\alpha - \gamma$ and $\alpha + \gamma$ at the intersection between the two shells.

A useful parameter defined by *Sumner et al.* [1990] is the effective solid angle of the mirror

$$E = 8\iint \sin\alpha \, \cos\alpha B(\alpha, w, z, i)d\phi d\alpha \quad (5)$$

The effective solid angle derived from the above analytical model is shown on Figure 2 (solid line) as a function of the grazing incidence of a mirror assumed
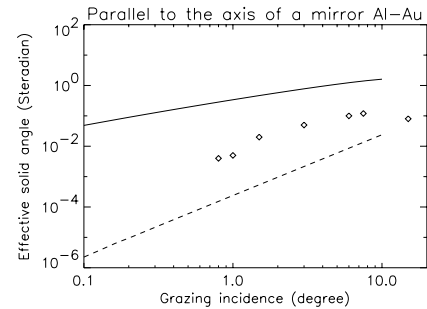

Figure 2. Effective solid angle derived from the above analytical model (solid line), the grazing incidence model of *Danner* [1993](dashed line) and a Monte-Carlo model (diamond).

to have one side in aluminium and one gold coated side. To compare with the results of *Sumner et al.* [1990] the length of the mirror has been modified according to the grazing incidence angle so as to just avoid direct segment of electrons without striking the mirror surface. The results obtained with the grazing incidence model of *Danner* [1993] (dashed line) and with the Monte-Carlo simulation of *Sumner et al.* [1990] (diamonds) are shown on the same graph. In the grazing incidence model, the electrons are assumed to propagate to the detector under grazing incidence only. The curves of Figure 2 show that this hypothesis leads to a strong underestimate of E (typically two orders of magnitude for one degree grazing incidence mirror system). The analytical model leads to a strong overestimate of E. The effect of the non-specular reflection especially on the Aluminium side may explain this discrepancy. The discrepancy between the analytical models and the Monte-Carlo based model is expected to be reduced for the high Z material and for the high grazing angle. In the first case because the reflection is more specular and in the second case because the absorption is more significant.

The derivation of E for three different X-ray experiments (including XMM [*Gondoin et al.* 1994]) is given in Table 1 and compared with the results of *Sumner et al.* [1990].

Table 1: Parallel and perpendicular flux coefficient.

Mission	SAX -WFC	ROSAT	XMM
Grazing incidence (deg)	0.3-0.6	5.6-9.3	0.3-0.7
η_1 (inner material)	0.22 (?)	0.22 (Al)	0.35 (Ni)
η_2 (coating material)	0.67 (Au)	0.67 (Au)	0.67 (Au)
L (m)	0.15	0.09	0.3
d (m)	10^{-3}	$2\,10^{-3}$	$2\,10^{-3}$
E (Ster)(Sumner et al.)	$8\,10^{-5}$	$2\,10^{-2}$	-
E (Ster)(this study)	0.1	0.2	0.09
$\int E_p dz$ (Ster·m)	0.03	0.02	0.01

4. FLUX PERPENDICULAR TO THE SHELL

The electron flux parallel to the mirror axis at depth z can be written:

$$F_2 = \iiint g(w) \sin\alpha \cos\phi A(\alpha, \phi, i) B(\alpha, w, z, i) d\phi d\alpha dw \quad (6)$$

In a similar way as above useful insight to the process is given by a parameter E_p

$$E_p = 8 \iint \sin\alpha \cos\phi B(\alpha, w, z, i) d\phi d\alpha \quad (7)$$

The parameter E_p is shown in Figure 3 as a function of z for a gold coated mirror of nickel. It is seen that E_p is a strongly decreasing function of z. It is actually decreasing by one order of magnitude over the first centimeter. Therefore, the particle induced X-ray background (PIB) is likely to be dominated by the first few centimeters of the mirror. The PIB is proportional to the integral of E_p over the mirror length. The value of $\int E_p dz$ is given in the last column of Table 1 for three different mirror missions.
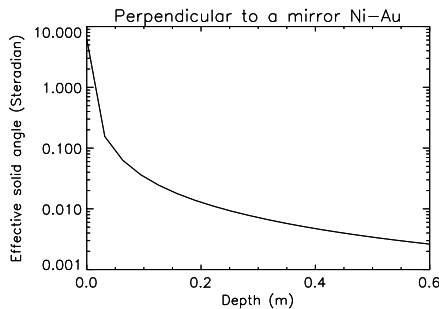

Figure 3. Effective solid angle for the flux perpendicular to a mirror shell derived from the analytical model.

5. FULL DERIVATION OF THE PARTICLE INDUCED BACKGROUND

In practice magnetic deflectors are used to deviate the electron flux exiting from the mirror. The main concern is therefore the particle induced X-ray background (PIB) generated by particle impact perpendicular to the shell. The general expression of the PIB due to the flux perpendicular to the shell is

$$\frac{\partial N}{\partial u} = \Sigma_i 2\pi r_i \iiiint g(w) \sin\alpha \cos\phi A(\alpha, \phi, i) B(\alpha, w, z, i)$$

$$C(\alpha, \phi, w, u, \epsilon) \pi D(z, i, u) d\phi d\alpha dz dw \quad (8)$$

where in addition to the terms already defined, i is the mirror number, r_i is the radius of mirror i, $C(\alpha, w, u, \epsilon)$ is the density of probability per sterardian and eV that a particle with a polar angle α and

energy w emits a photon with energy u and polar angle ϵ, and $D(z, i, u)$ is the density of probability that a photon emitted at location z inside mirror number i and with energy u reaches the detector.

The complete derivation of the PIB has been performed in the case of XMM mission [*Hilgers et al.* 1998]. To this end rather simple analytical models of the function A taking into account all the baffles and of the function D have been developed. A simple expression of the function C derived from simulations using the particle transport GEANT code [*GEANT*, 1993] could be found only in the case of the bremsstrahlung emission which represents a continuum component of the PIB. The line emissions are therefore not modelled. However, from the practical point of view they are affecting a much narrower spectral range than the continuum and they are easier to identify as such.

6. PARTICLE ENVIRONMENT

The distribution of the electron flux as measured with ISEE-2 spacecraft (cf Figure 4 and 5) appears very variable and high flux values for particles with energy of the order of 10 keV and above are observed in the whole domain explored by ISEE-2.
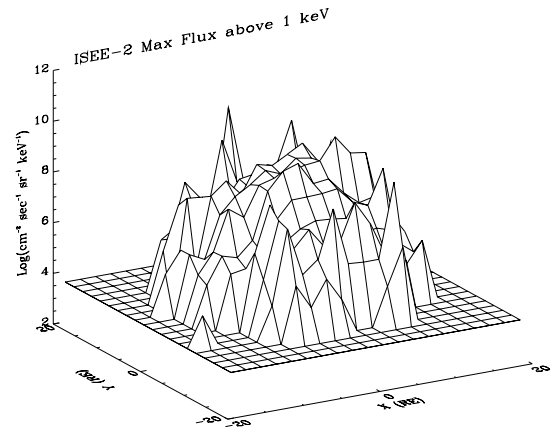

Figure 4. Maximum value of the electron flux derived from ISEE-2 as a function of the spacecraft position

The high flux values are expected to occur in the narrower domain identified as the plasmasheet. Close to Earth, the plasmasheet has a typical thickness of 10 to 12 R_E, further out the thickness decreases and is of about 6 to 8 R_E around $X_{GSE} = -20$ R_E [*Baumjohann* 1993]. The position of the plasmasheet, however, undergoes both regular and sporadic variation. First, there are diurnal and annual variations that are due to the change of the Earth magnetic dipole inclination with respect to the solar wind speed. Second, there are sporadic variations associated to storms and substorms during which the plasmasheet is thinning and expanding. For this study, a statistical model of the electron flux is derived directly from the distribution of the measurements of the flux in GSE
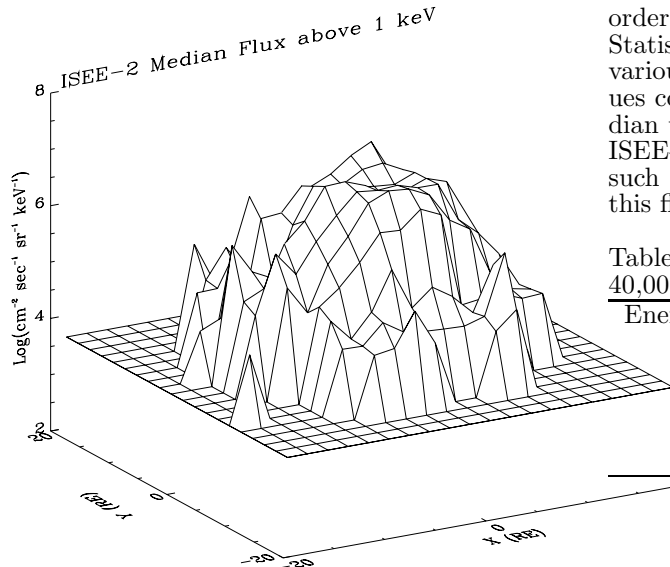
Figure 5. Median value of the electron flux derived from ISEE-2 as a function of the spacecraft position

order of magnitude as the actually measured flux. Statistical information of the flux integrated above various energy threshold are given Table 2. The values correspond to the maximum, minimum and median values observed above 40,000 km altitude with ISEE-2. The median flux is the value of the flux such that the observed probability of occurrence of this flux level or above is equal to 50%.

Table 2: Flux of electrons measured by ISEE-2 above 40,000 km altitude.

Energy threshold (keV)	Flux in $cm^{-2}sec^{-1}sr^{-1}$		
	Maximum	Median	Minimum
0.1	$1.4\,10^{10}$	$1.3\,10^5$	$4.9\,10^4$
1	$1.3\,10^{10}$	$1.2\,10^5$	$4.9\,10^4$
8	$7.2\,10^9$	$8.9\,10^4$	$4.8\,10^4$
10	$6.0\,10^9$	$8.1\,10^4$	$4.7\,10^4$

coordinate without discriminating diurnal or annual variations. Therefore, the model is providing an over estimate of the actual spreading of the plasmasheet at the time scale of XMM orbit. In order to improve such a model much more data would be needed to provide good statistics. A complete physical model of the plasmasheet is still a research topic. A summary of the current modelling effort is given by *Baumjohann* [1993] (cf also *Mälkki* [1998] and *Koskinen and Pulkkinen* [1998] for future plans).

Examples of spectra measured by ISEE-2 in the magnetosphere in the range 20-400 keV are shown in Figures 6 and 7.

In order to evaluate the particle induced X-ray background in the range 0.1 to 15 keV, the electron flux must be evaluated at energies down to 0.1 keV and above 400 keV. In the higher energy range, the electron flux is usually observed with a power law distribution [e.g., Baker et al., 1979]. Since the ISEE-2 spectra also exhibits such a power law, it was assumed that the same law holds for all energies above 400 keV. In the lower energy range, one would rather expect an exponential distribution because most of the particles are thermalized by wave particle interactions [e.g. Garrett, 1979]. An approximation of this exponential law is found by a fit of the lower energy channels of the ISEE-2 measurements. Eventually, the ISEE-2 spectra are fitted by the following analytical expressions,

$$g(w) = g_0 \exp\left(-\beta_1 w\right) \text{ for } w < 30 \text{ keV} \qquad (9)$$

and

$$g(w) = g_1 w^{-\beta_2} \text{ for } w > 30 \text{ keV}$$

Using these analytical fits, it is possible to extrapolate the integrated flux below 20 keV down to 0.1 keV and above 400 keV. Typically it was found that the part of the flux that was extrapolated is of the same
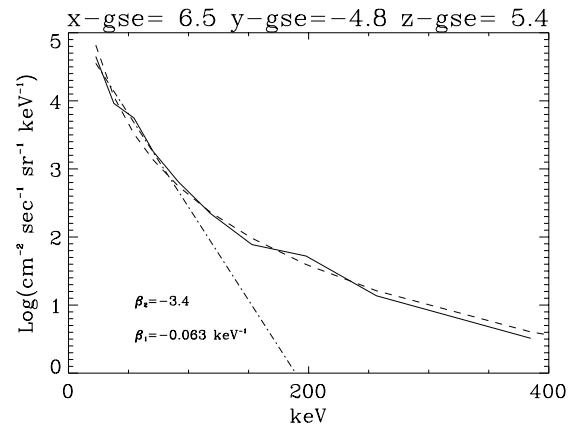

Figure 6. Electron spectra measured in the magnetosphere with ISEE-2. The dashed line represents a power law fit whereas the dotted-dashed line represents a fit of the lower energy range by an exponential.

Outside the magnetosphere there are two dominant background electron population: solar wind electrons with temperature of the order of 1 eV and density of a few tens of particles per cubic centimeter and relativistic Jovian electrons. The energy range of solar wind electrons is not relevant to this study. According to *Eraker* [1982], the background relativistic electrons at 1 AU can be fitted with a power law distribution as follows,

$$g(w) = g_2 w^{-\beta_3} \qquad (10)$$

with $g_2 = 2$ cm^{-2}sec^{-1}sr^{-1}keV^{-1} and $\beta_3 = 1.7$. This corresponds to an integrated flux above 1 keV equals to 2.9 cm^{-2}sec^{-1}sr^{-1}. In this study, the same law is used down to 0.1 keV because no information in the lower energy range was found. This assumption likely provides an overestimate of the flux in the lower energy range.

During solar magnetic field conjunction between Earth and Jupiter magnetospheres (observed with
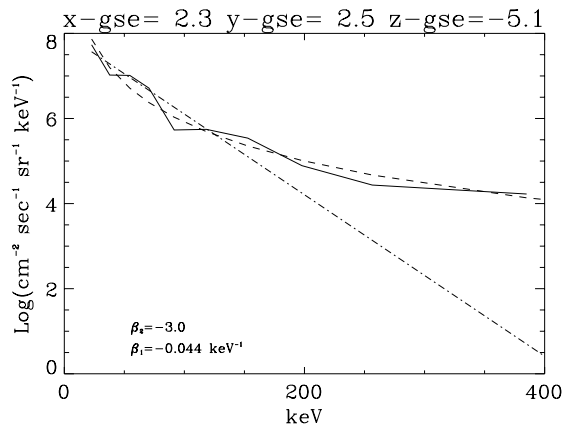
x−gse= 2.3 y−gse= 2.5 z−gse=−5.1

$\beta_e=-3.0$
$\beta_1=-0.044$ keV^{-1}

Figure 7. Same as before but with a much higher flux level observed with ISEE-2. The dashed line represents a power law fit whereas the dotted-dashed line represents a fit of the lower energy range by an exponential.

a period of about 30 months), enhancements of up to one order of magnitude above this level are observed [Chenette, 1980]. In addition to the above background relativistic electrons, there are also sporadic solar particle events, leading to relativistic electron flux enhancements by 2 to 3 orders of magnitude with also a higher spectral coefficient [e.g., Bothmer et al., 1997].

The median value of the bremsstrahlung induced background at 1 keV derived from equation (9) is shown as a function of the location in a GSE coordinate system in Figure 4. It can be seen that it is everywhere below the galactic X-ray background which is about 2 sec^{-1}keV^{-1} at this energy.
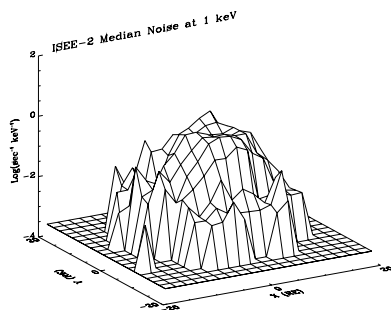

Figure 8. Median value of the bremsstrahlung induced background at 1 keV as deduced from ISEE-2.

Finally the median, lowest and highest value of the bremsstrahlung induced background at 1 keV is given over the whole domain explored by ISEE-2 but for altitudes above 40,000 km and for the interplanetary medium (e.g. solar wind). In the last column, the X-ray galactic background, XRB, is given.

Table 3: Prediction of X-ray background level in EPIC FOV

Photon Energy (keV)	$\partial N/\partial u$(sec^{-1}keV^{-1}) Magnetosphere			Cosmic background
	highest	median	lowest	
0.1	$2\,10^2$	$2\,10^{-2}$	$5\,10^{-3}$	≥ 10
0.2	$5\,10^2$	$5\,10^{-2}$	10^{-2}	≥ 10
1	10^3	10^{-1}	$4\,10^{-2}$	2.
8	$2\,10^2$	$2\,10^{-2}$	10^{-2}	$4\,10^{-2}$
10	6.	$8\,10^{-4}$	$5\,10^{-4}$	$2\,10^{-2}$

7. CONCLUSION

The above models provide simple analytical tools to derive the flux of ambient electrons propagating within X-ray mirror shells. They lead to an overestimate of the flux parallel to the axis (i.e. exiting from the mirror) compared to a more detailed but computationally heavy Monte-Carlo simulation. The estimate is likely to be more accurate for material with high atomic number. The flux perpendicular to the mirror shells has also been derived but no published information was found in the literature to compare with our results.

It has been shown that the combination of the particle transport models and an electron environment model could lead to an estimate of the bremsstrahlung induced background level in a detector. For instance, in the case of XMM, most of the time and over the whole energy range of the X-ray camera, the electron induced background is predicted to be significantly lower than the cosmic background. However, taking into account statistical fluctuations of the electron flux in the near Earth space environment it is found that instantaneous peak values of the bremsstrahlung induced background may overcome the cosmic background level. Therefore it is not excluded that measurements of very faint sources may be affected for long duration plasmasheet crossing by a X-ray observatory like XMM. For such missions a plasma instrument monitoring the electron environment in the range 100 - 10 keV would provide additional quality control of the X-ray data.

Future work is planned together with Rutherford Appleton Laboratory to use an extended data set in order to take into account actual typical plasma sheet crossing duration [SEDAT, 1998]. Furthermore, a strategy is needed to verify this model during XMM on orbit calibration phase. The radiation monitor located outside the spacecraft is designed for detecting essentially high energy particle (electron above 300 keV) and is likely not suitable to the detection of plasma sheet electrons. Other means may rely on the extrapolation of plasma sheet location from other measurements (e.g., Cluster, Image,...).

REFERENCES

Bothmer et al., *Solar energetic particle events and coronal mass ejections: new insights from SOHO*, in proceedings of the 31st ESLAB Symposium on Correlated Phenomena at the Sun, in the Heliosphere and in Geospace, ESA SP-415, ESTEC, Noordwijk, The Netherlands, 1998.

Danner, R., Charged particle induced background expected in X-ray detecting CCDs in highly eccentric earth orbits, *Experimental Astronomy, Vol. 4*, pp 105-116, 1993.

Eraker, J. H., Origins of the low-energy relativistic interplanetary electrons, *Astroph. J., 257*, 862-880, 1982.

GEANT, Detector Description and Simulation Tool, CERN Program Library Long Writeup W5013, CERN, Geneva, 1993.

Gondoin, P., D. de Chambure, K. van Katwijk, P. Kletzkine, D. Stramaccioni, B. Aschenbach, O. Citterio, R. Willingale, The XMM telescope, *SPIE Proc.2279*, pp.86-100, 1994.

Hilgers, A., P. Gondoin, P. Nieminen, and H. Evans, *X-ray background induced by electron bremsstrahlung emission in XMM telescopes: environmental input data and mathematical model*, ESA-WP-1942, Noordwijk, the Netherlands, Oct. 1998.

Loidl, G. D., E. Keppler, and R. Friedel, *Analysis of ISEE data*, Technical note 1 performed for ESTEC under Contract No 10725/94/NL/JG, April 1996.

SEDAT, Space Environment and Analysis Tools, http://www.wdc.rl.ac.uk/sedat/ .

Shimizu R., *Secondary electron yield with primary electron beam of kilo-electron volts*, J. Applied Phys., Vol. 45, pp 2107, 1974.

Sumner, T. J., J. J. Quenby, R. Lieu, J. Daniels, R. Willingale, and X. Moussas, *Susceptibility of soft X-ray grazing incidence telescopes to low energy electrons*, Mon. Not. R. Astr. Soc. , Vol. 238, pp 1047-1054, 1989.

Sumner, T. J. and R. Lieu, *Soft-electron background in X-ray telescopes using Wolter I grazing incidence optics in near-Earth orbits*, Optical Engineering, Vol. 29, No 10, pp 1291-1294, Oct. 1990.